

# Improving Continuous Sign Language Recognition with Consistency Constraints and Signer Removal

RONGLAI ZUO and BRIAN MAK, The Hong Kong University of Science and Technology, Hong Kong

Most deep-learning-based continuous sign language recognition (CSLR) models share a similar backbone consisting of a visual module, a sequential module, and an alignment module. However, due to limited training samples, a connectionist temporal classification loss may not train such CSLR backbones sufficiently. In this work, we propose three auxiliary tasks to enhance the CSLR backbones. The first task enhances the visual module, which is sensitive to the insufficient training problem, from the perspective of consistency. Specifically, since the information of sign languages is mainly included in signers' facial expressions and hand movements, a keypoint-guided spatial attention module is developed to enforce the visual module to focus on informative regions, *i.e.*, spatial attention consistency. Second, noticing that both the output features of the visual and sequential modules represent the same sentence, to better exploit the backbone's power, a sentence embedding consistency constraint is imposed between the visual and sequential modules to enhance the representation power of both features. We name the CSLR model trained with the above auxiliary tasks as consistency-enhanced CSLR, which performs well on signer-dependent datasets in which all signers appear during both training and testing. To make it more robust for the signer-independent setting, a signer removal module based on feature disentanglement is further proposed to remove signer information from the backbone. Extensive ablation studies are conducted to validate the effectiveness of these auxiliary tasks. More remarkably, with a transformer-based backbone, our model achieves state-of-the-art or competitive performance on five benchmarks, PHOENIX-2014, PHOENIX-2014-T, PHOENIX-2014-SI, CSL, and CSL-Daily.

CCS Concepts: • **Computing methodologies** → **Activity recognition and understanding**.

Additional Key Words and Phrases: continuous sign language recognition, auxiliary learning, signer-independent, feature disentanglement.

## ACM Reference Format:

Ronglai Zuo and Brian Mak. 2018. Improving Continuous Sign Language Recognition with Consistency Constraints and Signer Removal. *J. ACM* 37, 4, Article 111 (August 2018), 23 pages. <https://doi.org/XXXXXXX.XXXXXXX>

## 1 INTRODUCTION

Sign language is usually the principal communication method among hearing-impaired people. Sign language recognition (SLR) aims to transcribe sign languages into glosses (basic lexical units in a sign language), which is an important technology to bridge the communication gap between the normal-hearing and hearing-impaired people. According to the number of glosses in a sign sentence, SLR can be categorized into (a) isolated SLR (ISLR), in which each sign sentence consists of only a single gloss, and (b) continuous SLR (CSLR), in which each sign sentence may consist of multiple glosses. ISLR can be seen as a simple classification task, which becomes less popular in recent years. In this paper, we focus on CSLR which is more practical than its isolated counterpart.

Authors' address: Ronglai Zuo, rzuo@cse.ust.hk; Brian Mak, mak@cse.ust.hk, The Hong Kong University of Science and Technology, Hong Kong.

Permission to make digital or hard copies of all or part of this work for personal or classroom use is granted without fee provided that copies are not made or distributed for profit or commercial advantage and that copies bear this notice and the full citation on the first page. Copyrights for components of this work owned by others than ACM must be honored. Abstracting with credit is permitted. To copy otherwise, or republish, to post on servers or to redistribute to lists, requires prior specific permission and/or a fee. Request permissions from [permissions@acm.org](mailto:permissions@acm.org).

© 2018 Association for Computing Machinery.

0004-5411/2018/8-ART111 \$15.00

<https://doi.org/XXXXXXX.XXXXXXX>

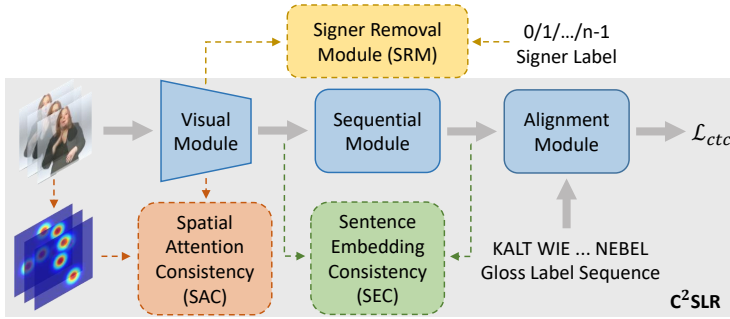


Fig. 1. An overview of the CSLR backbone and the three proposed auxiliary tasks. First, our SAC enforces the visual module to focus on informative regions by leveraging pose keypoints heatmaps. Second, our SEC aligns the visual and sequential features at the sentence level, which can enhance the representation power of both the features simultaneously. SAC and SEC constitute our preliminary work [77], consistency-enhanced CSLR ( $C^2$ SLR). In this work, we extend  $C^2$ SLR by developing a novel signer removal module based on feature disentanglement for signer-independent CSLR.

In recent years, more and more CSLR models are built using deep learning techniques because of their superior performance over traditional methods [43, 44, 75]. According to [44], the backbone of most deep-learning-based CSLR models is composed of three parts: a visual module, a sequential (contextual) module, and an alignment module. Within this framework, visual features are first extracted from sign videos by the visual module. After that, sequential and contextual information are modeled by the sequential module. Finally, due to the difference between the length of a sign video and its gloss label sequence, an alignment module is needed to align the sequential features with the gloss label sequence and yields its probability.

Usually, such CSLR backbones are trained with the connectionist temporal classification (CTC) [20] loss. However, since CSLR datasets are usually small, only using the CTC loss may not train the backbones sufficiently [13, 15, 23, 43, 50, 52, 75]. That is, the extracted features are not representative enough to be used to produce accurate recognition results. To relieve this issue, existing works can be roughly divided into two categories. First, [15] proposes a stage optimization strategy to iteratively refine the extracted features with the help of pseudo labels, which is widely adopted in [23, 50–52, 75]. However, it introduces more hyper-parameters and is time-consuming since the model needs to adapt to a different objective in each new stage [13]. As an alternative strategy, auxiliary learning can keep the whole model end-to-end trainable by just adding several auxiliary tasks [13, 43]. In this work, three novel auxiliary tasks are proposed to help train CSLR backbones.

Our first auxiliary task aims to enhance the visual module, which is important to feature extraction but sensitive to the insufficient training problem [15, 43, 75]. Since the information of sign languages is mainly included in signers' facial expressions and hand movements [25, 32, 75], signers' face and hands are treated as informative regions. Thus, to enrich the visual features, some CSLR models [48, 75, 76] leverage an off-the-shelf pose detector [8, 58] to locate the informative regions and then crop the feature maps to form a multi-stream architecture. However, this architecture will introduce extensive parameters since each stream processes its inputs independently and the cropping operation may overlook the rich information in the pose keypoints heatmaps. As shown in Figure 1, by visualizing the heatmaps, we find that they can reflect the importance of different spatial positions, which is similar to the idea of spatial attention. Thus, as shown in Figure 2, we insert a lightweight spatial attention module into the visual module and enforce the spatial

attention consistency (SAC) between the learned attention masks and pose keypoints heatmaps. In this way, the visual module can pay more attention to the informative regions.

Only enhancing the visual module may not fully exploit the power of the backbone. According to [23, 43], better performance can be obtained by explicitly enforcing the consistency between the visual and sequential modules. VAC [43] adopts a knowledge distillation loss between the two modules by treating the visual and sequential modules as a student-teacher pair. With a similar idea, SMKD [23] transfers knowledge by shared classifiers. Knowledge distillation can be treated as a kind of consistency since it is usually instantiated as the KL-divergence loss, a measurement of the distance between two probability distributions. Nevertheless, the above two methods have a common deficiency that they measure consistency at the frame level, *i.e.*, each frame has its own probability distribution. We think that it is inappropriate to enforce frame-level consistency since the sequential module is supposed to gather contextual information; otherwise, the sequential module may be dropped. Motivated by that both the visual and sequential features represent the same sentence, we propose the second auxiliary task: enforcing the sentence embedding consistency (SEC) between them. As shown in Figure 2, we build a lightweight sentence embedding extractor that can be jointly trained with the backbone, and then minimize the distance between positive sentence embedding pairs while maximizing the distance between negative pairs.

We name the CSLR model trained with SAC and SEC as consistency-enhanced CSLR (C<sup>2</sup>SLR). According to our experimental results (Table 8), with a transformer-based backbone, C<sup>2</sup>SLR can achieve satisfactory performance on signer-dependent datasets, in which all signers in the test set appear in the training set. However, as shown in Table 9a, C<sup>2</sup>SLR cannot outperform the state-of-the-art (SOTA) work on the more challenging but realistic signer-independent CSLR (SI-CSLR). Under the SI setting, since the signers in the test set are unseen during training, removing signer-specific information can make the model more robust to signer discrepancy. In this work, we further develop a signer removal module (SRM) based on the idea of feature disentanglement. More specifically, we first extract robust sentence-level signer embeddings with statistics pooling [57] to “distill” signer information, which is then dispelled from the backbone implicitly by a gradient reversal layer [17]. Finally, the SRM is trained with a signer classification loss. To the best of our knowledge, we are the first to develop a specific module for SI-CSLR<sup>1</sup>.

In summary, our main contributions are:

- We propose to enforce the consistency between the learned attention masks and pose keypoints heatmaps to enable the visual module to focus on informative regions.
- We propose to align the visual and sequential features at the sentence level to enhance the representation power of both features simultaneously.
- We propose a signer removal module from the idea of feature disentanglement to implicitly remove signer information from the backbone for SI-CSLR. To the best of our knowledge, we are the first to focus on this challenging setting.
- Extensive experiments are conducted to validate the effectiveness of the three auxiliary tasks. More remarkably, with a transformer-based backbone, our model can achieve SOTA or competitive performance on five benchmarks, while the whole model is trained in an end-to-end manner.

This work is an extension to our 2022 CVPR paper, C<sup>2</sup>SLR [77]. More specifically, we make the following new contributions:

- Besides the investigation on signer-dependent continuous sign language recognition (SD-CSLR) in the CVPR paper, we propose in this paper an additional signer removal module (SRM)

<sup>1</sup>Some works [15, 50] evaluate their methods on SI-CSLR datasets, but none of them propose any dedicated modules for the SI setting. [70] proposes a metric learning method to deal with the SI situation, but it focuses on ISLR.

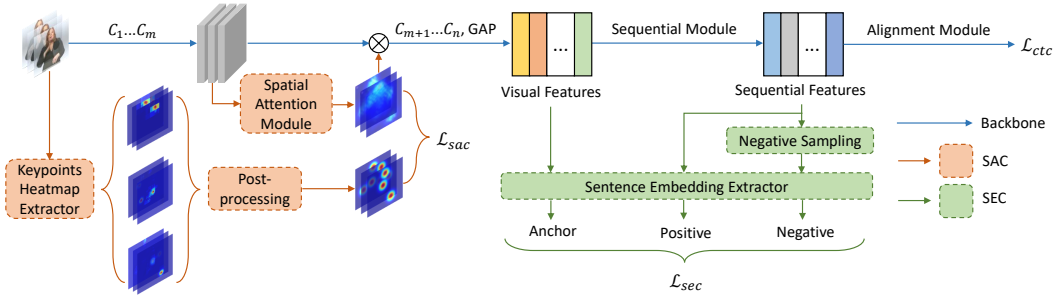


Fig. 2. An overview of our  $C^2$ SLR. For spatial attention consistency (SAC), we first insert a spatial attention module after the  $m$ -th convolution layer,  $C_m$ , of the visual module, and then guide it by pre-extracted pose keypoints heatmaps. For sentence embedding consistency (SEC), we extract the sentence embeddings of visual features, sequential features, and negative sequential features, respectively, and adopt a triplet loss to train the sentence embedding extractor along with the CSLR backbone. (GAP: global average pooling.)

to tackle the more challenging signer-independent continuous sign language recognition (SI-CSLR) problem. More specifically, the SRM is designed to remove signer information from the backbone for SI-CSLR based on feature disentanglement. To the best of our knowledge, we are the first to propose a dedicated module to deal with SI-CSLR.

- We successfully adapt statistics pooling to SI-CSLR to extract robust sentence-level signer embeddings for the SRM.
- We conduct sufficient ablation studies to validate the effectiveness of the SRM, and the combination of  $C^2$ SLR and SRM can achieve SOTA performance on an SI-CSLR benchmark.
- We also report additional experimental results of  $C^2$ SLR on the latest large-scale Chinese sign language dataset, CSL-Daily [73] with a vocabulary size of 2K and about 20K videos.

## 2 RELATED WORKS

### 2.1 Deep-learning-based CSLR

According to [44], most deep-learning-based CSLR backbones consist of a visual module (3D-CNNs [52, 74] or 2D-CNNs [23, 43, 75]), a sequential module (1D-CNNs [13, 21], RNNs [23, 43, 50, 52, 75], or Transformer [6, 44]), and an alignment module (CTC [23, 43, 75] or hidden Markov models [33, 36]). To relieve the insufficient training issue, [15] proposes a stage optimization strategy to iteratively refine the extracted features by using pseudo labels, which is widely adopted in [23, 50, 52, 75]. Based on it, [52] leverages LSTM to build an auxiliary decoder. SMKD [23] proposes a three-stage optimization strategy, which takes 100 epochs to train its model. In a more time-efficient way, VAC [43] proposes visual enhancement and visual alignment constraints over the frame-level probability distributions to enhance the visual module and to enforce the consistency between the visual and sequential modules, respectively, and the whole model is still end-to-end trainable. In this work, we enhance the visual module from a novel view of spatial attention consistency, and align the two modules at the sentence level to enforce their sentence embedding consistency.

Most of the existing works on CSLR only focus on the signer-dependent setting in which all signers in the test set appear during training. Few works pay attention to the signer-independent (SI) setting, which is more realistic but challenging as all test signers are unseen in the training set. In this work, we further propose a signer removal module based on feature disentanglement to make the model robust to signer discrepancy.

## 2.2 Spatial Attention

Spatial attention mechanism enables models to focus on specific positions, which is widely-adopted on many computer vision tasks, such as semantics segmentation [16], object detection [7, 65], and image classification [7, 26, 38, 61, 65]. However, the spatial attention module may not be well-trained with a single task-specific loss function. Leveraging external information to guide the spatial attention module can be a solution to this issue. In [11], the spatial attention module is guided by motion information for video captioning. [47] and [37] propose mask and relation guidance for occluded pedestrian detection and person re-identification, respectively. Interestingly, GALA [38] leverages click maps collected in a game to supervise the spatial attention module. In this work, we leverage pose keypoints heatmaps to guide the learning of the spatial attention module so that the visual module will focus on informative regions.

## 2.3 Sentence Embedding

Traditional methods [40, 46] simply feed the word embedding sequence into RNNs, and take the last hidden state (two for bidirectional RNNs) as the sentence embedding. Recently, many powerful sentence embedding extractors [9, 18, 53] are built on BERT [30]. However, it is difficult to use these methods in our work because (1) they are too large to be co-trained along with the backbone; (2) they are pretrained on spoken languages, which are totally different to sign languages represented by videos. In this work, we build a lightweight sentence embedding extractor that can be jointly trained with the CSLR backbone.

## 2.4 Feature Disentanglement

For SI-CSLR, each signer can be seen as a domain, and the key is to enable the model to generalize well to unseen domains, *i.e.*, the test signers. As an effective approach for domain generalization, feature disentanglement aims to decompose features into domain-invariant and domain-specific parts [62]. Adversarial learning has been widely adopted for feature disentanglement by treating the feature extractor as the generator and the domain classifier as the discriminator [14, 41, 67]. For example, [67] removes bias, *e.g.*, gender and race, for facial expression recognition by training a series of domain classifiers in an adversarial manner. Recently, [14] proposes a self-adversarial framework to remove gaze-irrelevant factors to boost gaze estimation performance. Another frequently-used feature disentanglement method is leveraging attention mechanism to highlight task-relevant features, and the residual features are treated as task-irrelevant ones. For example, [29] uses a channel attention module to remove style information for person re-identification, and [28] uses both spatial and channel attention to remove age-related features for face recognition. However, adversarial learning is usually complicated as the generator and discriminator are trained iteratively, and the attention modules would introduce extra parameters. In this work, we adopt the gradient reversal (GR) layer [17] that reverses the gradient coming from the domain (signer) classification loss when the back-propagation process arrives at the feature extractor (CSLR backbone) while keeping the gradient of the domain classifier unchanged. It shares a similar idea with adversarial learning, but it is totally end-to-end and introduces no extra parameters compared to attention-based methods. Thus, we believe it can serve as a simple baseline for future research on SI-CSLR.

# 3 OUR PROPOSED METHOD

## 3.1 Framework Overview

The blue arrows in Figure 2 show the three components of the CSLR backbone: visual module, sequential module, and alignment module. Taking a sign video with  $T$  RGB frames  $\mathbf{x} = \{\mathbf{x}_t\}_{t=1}^T \in$

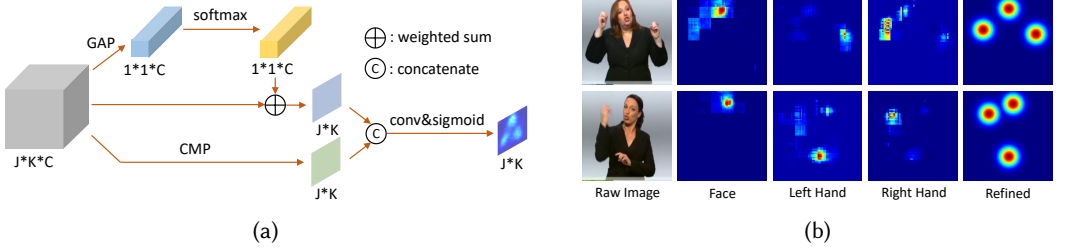


Fig. 3. (a) The architecture of our spatial attention module. ( $J \times K \times C$ : the size of the input feature maps, GAP: global average pooling, CMP: channel-wise max pooling. (b) Two examples of the original and refined heatmaps.

$\mathbb{R}^{T \times H \times W \times 3}$  as input, the visual module, which simply consists of several 2D-CNN<sup>2</sup> layers ( $C_1, \dots, C_n$ ) followed by a global average pooling (GAP) layer, first extracts visual features  $\mathbf{v} = \{\mathbf{v}_t\}_{t=1}^T \in \mathbb{R}^{T \times d}$ . The sequential features  $\mathbf{s} = \{\mathbf{s}_t\}_{t=1}^T \in \mathbb{R}^{T \times d}$  will be further extracted by the sequential module. Finally, the alignment module computes the probability of the gloss label sequence  $p(\mathbf{y}|\mathbf{x})$  based on the widely-adopted CTC [20], where  $\mathbf{y} = \{y_i\}_{i=1}^N$  and  $N$  denotes the length of the gloss sequence.

### 3.2 Spatial Attention Consistency (SAC)

Signers' facial expressions and hand movements are two major clues of sign languages [32, 75]. Thus, it is reasonable to expect the visual module can focus on signers' face and hands, *i.e.*, informative regions (IRs). From this view, we insert a spatial attention module into the visual module and enforce the consistency between the learned attention masks and keypoints heatmaps. Since SAC is applied to all frames in the same way, we will omit the time steps in the formulation below.

**3.2.1 Spatial Attention Module.** We build our spatial attention module based on CBAM [65] due to its simplicity and effectiveness. As shown in Figure 3a, we first pick the most informative channel via a channel-wise max pooling (CMP) operation:

$$\mathbf{M}_1 = f_{CMP}(\mathbf{F}) \in \mathbb{R}^{J \times K \times 1}, \quad (1)$$

where  $\mathbf{M}_1$  is the squeezed feature map by CMP, and  $\mathbf{F} \in \mathbb{R}^{J \times K \times C}$  is the input feature maps.

Besides CMP, CBAM also squeezes the feature maps with an average pooling operation along the channel dimension. However, we propose to dynamically weight the importance of each channel. As shown in Figure 3a, we first conduct global average pooling (GAP) over  $\mathbf{F}$  to gather global spatial information. Then the channel weights  $\mathbf{E} \in (0, 1)^{1 \times 1 \times C}$  are simply generated by a channel-wise softmax layer. By a weighted sum along the channel dimension, we can generate another squeezed feature map  $\mathbf{M}_2$ :

$$\mathbf{M}_2 = \mathbf{F} \oplus \mathbf{E} = \sum_{i=1}^C \mathbf{F}_i \cdot \mathbf{E}_i \in \mathbb{R}^{J \times K \times 1}, \quad (2)$$

Finally, the spatial attention mask  $\mathbf{M}$  is generated as:

$$\mathbf{M} = \sigma(f_{conv}(cat(\mathbf{M}_1, \mathbf{M}_2))) \in (0, 1)^{J \times K}, \quad (3)$$

where  $\sigma(\cdot)$  is the sigmoid function,  $f_{conv}(\cdot)$  is a 2D-CNN layer with a kernel size of  $7 \times 7$ , and  $cat(\cdot, \cdot)$  is a channel-wise concatenation operation. The output feature maps will be a product between  $\mathbf{F}$  and  $\mathbf{M}$ . In this way, important positions can be highlighted while trivial ones can be suppressed.

<sup>2</sup>We only consider visual modules based on 2D-CNNs since a recent survey [1] shows that 3D-CNNs cannot provide as precise gloss boundaries as 2D-CNNs, and lead to worse performance.

It should be noted that our channel weights are similar to the channel attention module in CBAM, but ours introduces no extra parameters and can even outperform the vanilla CBAM according to our ablation studies in Table 2.

**3.2.2 Keypoints Heatmap Extractor.** Simply training the spatial attention module with the backbone may lead to sub-optimal solutions. Given the prior knowledge that signers' faces and hands are informative regions (IRs), we guide the spatial attention module with keypoints heatmaps extracted by the pretrained HRNet [2, 58]. Specifically, we first normalize the raw outputs of HRNet linearly to obtain the original heatmaps:

$$\mathbf{H}_o^i = \frac{f_H^i(\mathbf{I}) - \min f_H^i(\mathbf{I})}{\max f_H^i(\mathbf{I}) - \min f_H^i(\mathbf{I})} \in [0, 1]^{H \times W}, \quad (4)$$

where  $\mathbf{I}$  is the raw RGB frame,  $f_H(\cdot)$  is the pretrained HRNet, and  $i \in \{1, 2, 3\}$  denotes the face, left hand, and right hand, respectively.

**3.2.3 Post-processing.** There are some defects in the original heatmaps although they can roughly highlight the positions of IRs. As shown in Figure 3b, some trivial regions, e.g., the top of the face heatmap in the first row and the middle part of the left hand heatmap in the second row, may receive high activation values. Besides, some highlighted regions, e.g., both of the face heatmaps in Figure 3b, may not cover the IRs entirely. In addition, there is usually a mismatch between the fixed heatmap resolution of the pretrained HRNet and that of the spatial attention masks. Below we will elaborate our heatmap post-processing module that corrects the mismatch.

We first locate the center of each IR from the original heatmaps via a simple argmax operation:  $(x_i, y_i) = \operatorname{argmax} \mathbf{H}_o^i$ . To fit different resolutions of spatial attention masks, we normalize the center as  $(\hat{x}_i, \hat{y}_i) = (\frac{x_i}{H-1}, \frac{y_i}{W-1})$ . Suppose the spatial attention masks have a common resolution of  $J \times K$ , then a Gaussian-like refined keypoints heatmap is generated for each IR to reduce unwanted noise:

$$\mathbf{H}_r^i(a, b) = \exp\left(-\frac{1}{2} \left( \frac{(a - \hat{c}_i^x)^2}{(J/\gamma_x)^2} + \frac{(b - \hat{c}_i^y)^2}{(K/\gamma_y)^2} \right)\right), \quad (5)$$

where  $0 \leq a < J, 0 \leq b < K$ .  $(\hat{c}_i^x, \hat{c}_i^y) = (\hat{x}_i(J-1), \hat{y}_i(K-1))$ , which denotes the transformed center for each IR under the resolution  $J \times K$ .  $\gamma_x$  and  $\gamma_y$  are two hyper-parameters to control the scale of the highlighted regions. In real practice, we set  $\gamma_x = \gamma_y$ . Finally, we merge the three processed IR heatmaps into a single one:  $\mathbf{H}_r = \max_i \mathbf{H}_r^i \in (0, 1)^{J \times K}$ .

**3.2.4 SAC Loss.** The spatial attention module is guided by the refined keypoints heatmaps via the SAC loss<sup>3</sup>:

$$\mathcal{L}_{sac} = \frac{1}{J \times K} \|\mathbf{M} - \mathbf{H}_r\|_2^2. \quad (6)$$

### 3.3 Sentence Embedding Consistency (SEC)

Some works [23, 43] find that enforcing the consistency between the visual and sequential features can enhance their representation power, and lead to better performance. Different from [23, 43] that measure their consistency at the frame level, we impose a sentence embedding consistency between them.

<sup>3</sup>For implementation, we further compute the average of  $\mathcal{L}_{sac}$  over all time steps.

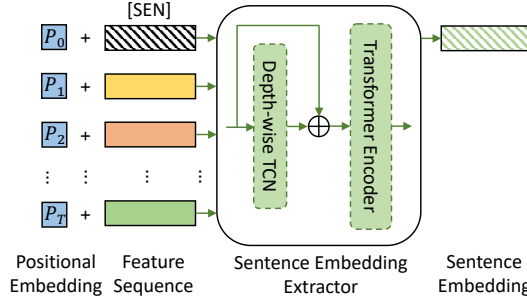


Fig. 4. The workflow of sentence embedding extraction. We omit LayerNorm [3] for simplicity.

**3.3.1 Sentence Embedding Extractor (SEE).** Within a sign video, each gloss consists of only a few frames. We believe a good SEE for sign languages should take local contexts into consideration. As shown in Figure 4, our SEE is built on QANet [71], which consists of a depth-wise temporal convolution network (TCN) layer and a transformer encoder layer. The depth-wise TCN first extracts local contextual information from the frame-level feature sequence, then the transformer encoder models global contexts by its inner self-attention module.

Similar to the class token in BERT [30], we first prepend a learnable sentence embedding token, [SEN], to the sequential features  $\mathbf{s} \in \mathbb{R}^{T \times d}$  defined in Section 3.1:

$$\mathbf{s}' = \text{cat}([\text{SEN}], \mathbf{s}) \in \mathbb{R}^{(T+1) \times d}. \quad (7)$$

The input of the SEE is the summation of the feature sequence and the positional embeddings [60]; i.e.,  $\mathbf{s}'' = \mathbf{s}' + \mathbf{P}$ , where  $\mathbf{P} \in \mathbb{R}^{(T+1) \times d}$ .

Within the SEE, the depth-wise TCN [66] layer first models local contexts with a residual shortcut:  $\mathbf{s}_l'' = f_{TCN}(\mathbf{s}'') + \mathbf{s}''$ . Then the transformer encoder layer gathers information from all time steps to get the sentence embedding:

$$\mathbf{E}_{sen}^s = f_{TF}(\mathbf{s}_l'') = \sum_{i=0}^T w_i \mathbf{s}_i'' \in \mathbb{R}^d, \quad (8)$$

where  $w_i$  are the learned weights by the self-attention module in the transformer encoder. We can also get the sentence embedding of visual features,  $\mathbf{E}_{sen}^v$ , in the same way.

**3.3.2 Negative Sampling.** Directly minimizing the distance between  $\mathbf{E}_{sen}^s$  and  $\mathbf{E}_{sen}^v$  will result in trivial solutions. For example, if the parameters of SEE are all zeros, then the outputs of SEE will always be the same. A simple way to address this issue is introducing negative samples. In this work, we follow the common practice [24, 45, 54, 69] and sample another video from the mini-batch and take its sequential features as the negative sample. Note that most CSLR models [23, 43, 75, 76] are trained with a batch size of 2, and our negative sampling strategy will degenerate to swapping under this setting:

$$(\text{neg}(\mathbf{B}[0]), \text{neg}(\mathbf{B}[1])) = (\mathbf{B}[1], \mathbf{B}[0]), \quad (9)$$

where  $\mathbf{B} \in \mathbb{R}^{2 \times T \times d}$  is a mini-batch of the sequential features, and  $\text{neg}(\mathbf{B}[\cdot])$  denotes the corresponding negative sample.

**3.3.3 SEC Loss.** We implement SEC loss as a triplet loss [54] and minimize the distances between the sentence embeddings computed from the visual and sequential features of the same sentence,



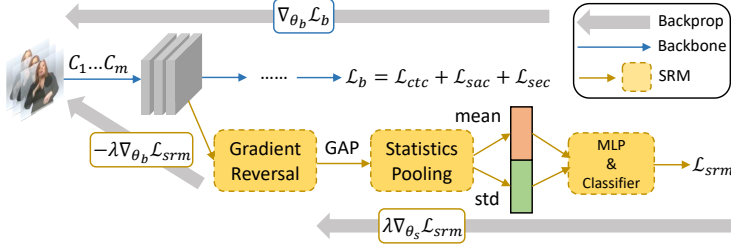


Fig. 5. The workflow of our signer removal module (SRM). We insert the SRM after the  $m$ -th CNN layer,  $C_m$ . The loss of  $C^2$ SLR,  $\mathcal{L}_b$ , which is a sum of the CTC, SAC, and SEC losses, is used to train the backbone parameters  $\theta_b$ . The signer classification loss  $\mathcal{L}_{srm}$  is used to train the SRM parameters  $\theta_s$  as usual, while the gradient coming from  $\mathcal{L}_{srm}$  will be reversed for  $\theta_b$ .  $\lambda$  is the loss weight for  $\mathcal{L}_{srm}$ .

while maximizing the distances between those from different sentences:

$$\mathcal{L}_{sec} = \max\{d(\mathbf{E}_{sen}^v, \mathbf{E}_{sen}^s) - d(\mathbf{E}_{sen}^v, \text{neg}(\mathbf{E}_{sen}^s)) + \alpha, 0\}, \quad (10)$$

where  $d(\mathbf{x}_1, \mathbf{x}_2) = 1 - \frac{\mathbf{x}_1 \cdot \mathbf{x}_2}{\|\mathbf{x}_1\|_2 \cdot \|\mathbf{x}_2\|_2}$ ;  $\{\mathbf{E}_{sen}^v, \mathbf{E}_{sen}^s\}$  are sentence embeddings of visual and sequential features from the same sentence;  $\{\mathbf{E}_{sen}^v, \text{neg}(\mathbf{E}_{sen}^s)\}$  are sentence embeddings of visual and sequential features from different sentences, and we treat the sentence embedding of the sequential features from a different sentence as the negative sample  $\text{neg}(\mathbf{E}_{sen}^s)$ ;  $\alpha$  is the margin.

### 3.4 Signer Removal Module (SRM)

To remove signer information from CSLR backbones, we further develop a signer removal module (SRM) based on statistics pooling and gradient reversal as shown in Figure 5.

**3.4.1 Signer Embeddings.** We first extract signer embeddings to “distill” signer information before dispelling it. A naïve method is simply feeding the frame-level features into an MLP, and treat the outputs of MLP as signer embeddings. In this work, motivated by the superior performance of x-vectors [57] in speaker recognition, we leverage statistics pooling to obtain more robust sentence-level signer embeddings.

Specifically, we first feed the intermediate visual features  $\mathbf{F} \in \mathbb{R}^{T \times J \times K \times C}$  into a global average pooling layer to squeeze the spatial dimension and obtain frame-level features<sup>4</sup>  $\mathbf{F}_s \in \mathbb{R}^{T \times C}$ . Then a statistics pooling (SP) layer is used to aggregate frame-level information:

$$\mathbf{F}_s^{SP} = \text{cat}(\mathbf{F}_s^{\text{mean}}, \mathbf{F}_s^{\text{std}}) \in \mathbb{R}^{2C}, \quad (11)$$

where  $\mathbf{F}_s^{\text{mean}} \in \mathbb{R}^C$  and  $\mathbf{F}_s^{\text{std}} \in \mathbb{R}^C$  are the temporal mean and standard deviation of  $\mathbf{F}_s$ , respectively. In this way,  $\mathbf{F}_s^{SP}$  is capable to capture signer characteristics over the entire video instead of at the frame-level.

After that, a simple two-layer MLP with rectified linear unit (ReLU) function is used to project the statistics into the signer embedding space:

$$\mathbf{E}_{sig} = \text{ReLU}(\mathbf{W}_2 \text{ReLU}(\mathbf{W}_1 \mathbf{F}_s^{SP} + \mathbf{b}_1) + \mathbf{b}_2) \in \mathbb{R}^C, \quad (12)$$

where  $\mathbf{W}_1 \in \mathbb{R}^{C \times 2C}$ ,  $\mathbf{b}_1 \in \mathbb{R}^C$ ,  $\mathbf{W}_2 \in \mathbb{R}^{C \times C}$ ,  $\mathbf{b}_2 \in \mathbb{R}^C$  represent the two-layer MLP.

Finally, the signer embeddings  $\mathbf{E}_{sig}$  are fed into a classifier to yield signer probabilities  $\mathbf{p}_{sig} \in (0, 1)^{N_{sig}}$ , where  $N_{sig}$  denotes the number of signers. The SRM is trained with the signer classification

<sup>4</sup>Here we misuse the notation  $\mathbf{F}$  in Eq.1.

loss, which is simply a cross-entropy loss:

$$\mathcal{L}_{srm} = -\log p_{sig}^i \quad (13)$$

where  $i$  is the label of the signer.

**3.4.2 Gradient Reversal.** If the CSLR backbone is jointly trained with  $\mathcal{L}_{srm}$ , it will become the multi-task learning, which, however, cannot promise removing the signer information from the backbone. In this work, we treat each signer as a domain and formulate SI-CSLR as a domain generalization problem in which no test signers are seen during training. The gradient reversal layer was proposed in [17] to address the domain generalization problem by learning features that are discriminative to the main classification task while indiscriminate to the domain gap. More specifically, according to [17], denoting the parameters of the feature extractor, label predictor, and domain classifier as  $\theta_f$ ,  $\theta_y$ , and  $\theta_d$ , respectively, the optimization of these parameters can be formulated as:

$$\begin{aligned} \theta_f &\leftarrow \text{optimizer}(\theta_f, \nabla_{\theta_f} \mathcal{L}_y, -\lambda \nabla_{\theta_f} \mathcal{L}_d, \eta), \\ \theta_y &\leftarrow \text{optimizer}(\theta_y, \nabla_{\theta_y} \mathcal{L}_y, \eta), \\ \theta_d &\leftarrow \text{optimizer}(\theta_d, \lambda \nabla_{\theta_d} \mathcal{L}_d, \eta), \end{aligned} \quad (14)$$

where  $\mathcal{L}_y$  and  $\mathcal{L}_d$  are the main classification and domain classification losses, respectively,  $\lambda$  is the loss weight for  $\mathcal{L}_d$ , and  $\eta$  is the learning rate.

We adapt Eq. 14 by instantiating  $\mathcal{L}_y$  and  $\mathcal{L}_d$  as the backbone training loss  $\mathcal{L}_b$  and signer classification loss  $\mathcal{L}_{srm}$ , which are illustrated in Figure 5, respectively. We also merge  $\theta_f$  and  $\theta_y$  as  $\theta_b$  to denote the parameters of the backbone, and use  $\theta_s$  to represent the parameters of the SRM. The new optimization process can be formulated as:

$$\begin{aligned} \theta_b &\leftarrow \text{optimizer}(\theta_b, \nabla_{\theta_b} \mathcal{L}_b, -\lambda \nabla_{\theta_b} \mathcal{L}_{srm}, \eta), \\ \theta_s &\leftarrow \text{optimizer}(\theta_s, \lambda \nabla_{\theta_s} \mathcal{L}_{srm}, \eta). \end{aligned} \quad (15)$$

As a result, the SRM itself is trained with  $\mathcal{L}_{srm}$  as usual, but the backbone is trained “reversely” so that the extracted features cannot discriminate signers, and the signer information is implicitly removed. We empirically validate the effectiveness of the SRM on two challenging SI-CSLR benchmarks, establishing a strong baseline for future works on SI-CSLR.

### 3.5 Alignment Module and Loss Function

We follow recent works [23, 43, 50, 75] to adopt CTC-based alignment module. It yields a label for each frame which may be a repeating label or a special blank symbol. CTC assumes that the model output at each time step is conditionally independent of each other. Given an input sequence  $\mathbf{x}$ , the conditional probability of a label sequence  $\phi = \{\phi_i\}_{i=1}^T$ , where  $\phi_i \in \mathcal{V} \cup \{\text{blank}\}$  and  $\mathcal{V}$  is the vocabulary of glosses, can be estimated by:

$$p(\phi|\mathbf{x}) = \prod_{i=1}^T p(\phi_i|\mathbf{x}), \quad (16)$$

where  $p(\phi_i|\mathbf{x})$  is the frame-level gloss probabilities generated by a classifier. The final probability of the gloss label sequence is the summation of all feasible alignments:

$$p(\mathbf{y}|\mathbf{x}) = \sum_{\phi \in \mathcal{G}^{-1}(\mathbf{y})} p(\phi|\mathbf{x}), \quad (17)$$

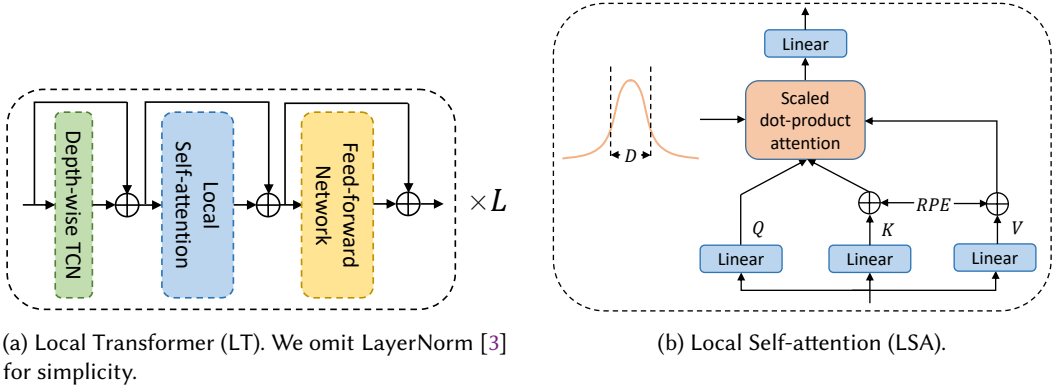


Fig. 6. We propose a strong sequential module, local transformer. It is based on QANet [71], which validates the effectiveness of combining TCNs with self-attention. The difference is that we further leverage Gaussian bias [42, 68] to introduce local contexts into the self-attention module, *i.e.*, local self-attention. ( $L$ : number of LT layers, which is set to 2 as default;  $RPE$ : relative positional encoding [55];  $D$ : window size of the Gaussian bias.)

where  $\mathcal{G}$  is a mapping function to remove repeats and blank symbols in  $\phi$ , and  $\mathcal{G}^{-1}$  is its inverse mapping. Then the CTC loss is defined as:

$$\mathcal{L}_{ctc} = -\log p(\mathbf{y}|\mathbf{x}). \quad (18)$$

Finally, the overall loss function is a combination of the CTC, SAC, SEC, and signer classification losses:

$$\mathcal{L} = \underbrace{\mathcal{L}_{ctc} + \mathcal{L}_{sac} + \mathcal{L}_{sec}}_{\mathcal{L}_b} + \lambda \mathcal{L}_{srm}, \quad (19)$$

where  $\lambda = 0$  for signer-dependent datasets, and  $\lambda > 0$  for signer-independent ones.

### 3.6 A Strong Sequential Module: Local Transformer

The sequential module is an important component of the CSLR backbone. Most existing CSLR works adopt globally-guided architectures, *e.g.*, BiLSTM [50, 52] and vanilla Transformer [6, 44], for sequence modeling due to their strong capability of capturing long-term temporal dependencies. However, within a sign video, each gloss is short, consisting of only a few frames. This can explain why a locally-guided architecture, such as TCNs, can also achieve excellent performance [13]. In this subsection, we will elaborate a mixed architecture, Local Transformer (LT), which can leverage both global and local contexts for sequence modeling for CSLR.

Figure 6a shows the architecture of LT. Each LT layer consists of a depth-wise TCN layer, a local self-attention (LSA) layer, and a feed-forward network. Since the depth-wise TCN layer and the feed-forward network are the same as those used in [60, 71], below we will only give the formulation of the LSA.

As shown in Figure 6b, three linear layers first project the input feature sequence  $\mathbf{A} \in \mathbb{R}^{T \times d}$  into queries  $\mathbf{Q} \in \mathbb{R}^{T \times d}$ , keys  $\mathbf{K} \in \mathbb{R}^{T \times d}$ , and values  $\mathbf{V} \in \mathbb{R}^{T \times d}$ , respectively. We then split  $\mathbf{Q}, \mathbf{K}, \mathbf{V}$  into  $\{\mathbf{Q}^h\}_{h=1}^{N_h}, \{\mathbf{K}^h\}_{h=1}^{N_h}, \{\mathbf{V}^h\}_{h=1}^{N_h}$ , respectively, for multi-head self-attention as [60], where  $\mathbf{Q}^h, \mathbf{K}^h, \mathbf{V}^h \in \mathbb{R}^{T \times d/N_h}$  and  $N_h$  is the number of heads. The attention scores for each head can be obtained by the

scaled dot-product attention as follows:

$$\text{ATT} = \left\{ \frac{(\mathbf{Q}^h)(\mathbf{K}^h)^T}{\sqrt{d/N_h}} \right\}_{h=1}^{N_h} \in \mathbb{R}^{N_h \times T \times T}. \quad (20)$$

The vanilla self-attention treats each position equally. To emphasize local contexts, we adopt Gaussian bias [42, 68] to weaken the interactions between distant query-key (QK) pairs. Given a QK pair  $(\mathbf{q}_i^h, \mathbf{k}_j^h)$ , the Gaussian bias (GB) is defined as:

$$\text{GB}_{ij}^h = -\frac{(j-i)^2}{2\sigma^2}, \quad (21)$$

where  $\sigma = \frac{D}{2}$ , and  $D$  is the window size of the Gaussian bias [42]. Note that although we can assign Gaussian bias with a different value of  $D$  for each head, we find that a common Gaussian bias among all heads suffices to boost the performance of transformer significantly. The final attention weights for each value vector are obtained from a softmax layer, and the output of the LSA is:

$$\begin{cases} \mathbf{O}^h = \text{softmax}(\text{ATT}^h + \text{GB}^h)\mathbf{V}^h \\ \mathbf{O}^{\text{LSA}} = \text{cat}(\{\mathbf{O}^h\}_{h=1}^{N_h})\mathbf{W}^O \in \mathbb{R}^{T \times d}, \end{cases} \quad (22)$$

where  $\mathbf{W}^O \in \mathbb{R}^{d \times d}$  denotes the output linear layer.

We intuitively set  $D$  as the average ratio of frame length to gloss length:  $D = \frac{1}{|tr|} \sum_{i=1}^{|tr|} \frac{T_i}{N_i}$ , where  $|tr|$  is the number of training samples, based on the idea that a good window size should reflect the average frame length of a gloss. More specifically,  $D = 6.3, 15.8, 5.0$  for the PHOENIX datasets, CSL, and CSL-Daily, respectively.

## 4 EXPERIMENTS

### 4.1 Datasets and Evaluation Metric

**4.1.1 Datasets.** We evaluate our method on three signer-dependent datasets (PHOENIX-2014, PHOENIX-2014-T, and CSL-Daily) and two signer-independent datasets (PHOENIX-2014-SI and CSL).

**PHOENIX-2014** [34] is a German CSLR dataset with a vocabulary size of 1081. There are 5672, 540, and 629 videos performed by 9 signers in the training, development (dev), and test set, respectively.

**PHOENIX-2014-T** [5] is an extension of PHOENIX-2014 with a vocabulary size of 1085. There are 7096, 519, and 642 videos performed by 9 signers in the training, dev, and test set, respectively.

**CSL-Daily** [73] is the latest large-scale Chinese sign language dataset consisting of 18401, 1077, 1176 videos performed by 10 signers in the training, dev, and test set, respectively. Its vocabulary size is 2000.

**PHOENIX-2014-SI** [34] is the signer-independent version of PHOENIX-2014 consisting of 4376, 111, and 180 videos in the training, dev, and test set, respectively. It has 8 signers for training, and leaves the remaining one for validation and test.

**CSL** [27, 52, 74] is a Chinese CSLR dataset consisting of 4000 and 1000 videos in the training and test set, respectively, with a vocabulary size of 178. We follow [13, 43] to conduct experiments on its signer-independent split in which 40 signers only appear in training while the remaining 10 signers only appear in testing.

Compared to some widely-adopted datasets in action recognition, e.g., Kinetics-600 [10] with 500K videos and Something-Something v2 [19] with 169K videos, the size of these sign language datasets are quite small. This can also explain why some specific training strategies, e.g., stage optimization and auxiliary training, are suggested necessary for CSLR before.

**4.1.2 Evaluation Metric.** We use word error rate (WER) to measure the dissimilarity between two sequences.

$$\text{WER} = \frac{\#\text{deletions} + \#\text{substitutions} + \#\text{insertions}}{\#\text{glosses in label}} \quad (23)$$

The official evaluation scripts provided by each dataset are used for measuring the WER.

## 4.2 Implementation Details

**4.2.1 Data Augmentation.** We first resize RGB frames to  $256 \times 256$  and then crop them to  $224 \times 224$ . Stochastic frame dropping (SFD) [44] with a dropping ratio of 50% is adopted for the PHOENIX datasets. Since videos in CSL and CSL-Daily are much longer, we adopt a *seg-and-drop* strategy that first segments the videos into short clips consisting of only two frames, and then one frame is randomly dropped from each clip. In this way, the processed videos only consist of half of the original frames while most information can be kept. After that, we further randomly drop 40% frames using SFD from these processed videos.

**4.2.2 Backbones and Hyper-parameters.** We choose the following three representative backbones to validate the effectiveness of our method.

- VGG11+TCN+BiLSTM (VTB). It is widely adopted in some recent works [43, 75]. VGG11 [56] is used as the visual module, and the sequential module is composed of the TCN and BiLSTM to capture both local and global contexts.
- CNN+TCN (CT). This lightweight backbone only consists of a 9-layer 2D-CNN and a 3-layer TCN, which is proposed in [13].
- VGG11+Local Transformer (VLT). The sequential module is a 2-layer local transformer encoder described in Section 3.6.

We set the number of output channels of the TCN layers in CT and VTB to 512 and the number of hidden units of BiLSTM in VTB to  $2 \times 256$  to match the channel dimensions of the visual and sequential features. These modifications lead to comparable WERs with those reported in the original papers [13, 75]. We insert the spatial attention module after the 5th CNN layer as a trade-off between heatmap resolution and GPU memory limitation. In terms of post-processing, we set  $\gamma_x = \gamma_y = 14$  according to the experimental results in Section 4.3.6. The kernel size of the depth-wise TCN layer in both our SEE and VLT backbone is set to 5, which is the same as in [71]. The margin  $\alpha$  in Eq. 10 is set to 2, which is the maximum difference between the negative and positive distance with a cosine distance function. Regarding the signer removal module, we also put it after the 5th CNN layer, and the weight for  $\mathcal{L}_{srm}$ ,  $\lambda$ , is set to 0.75 by default.

**4.2.3 Training.** Following recent works [23, 43, 75], all models are trained with a batch size of 2. We adopt an Adam optimizer [31] with an initial learning rate of  $1 \times 10^{-4}$  and a weight decay factor of  $1 \times 10^{-4}$ . We empirically find that  $\mathcal{L}_{sec}$  decreases much faster than  $\mathcal{L}_{ctc}$ , thus we multiply the learning rate of the SEE with a factor of 0.1/0.01/0.1 for the three backbones, respectively, to match the training pace of the backbone and SEE. As in [6], we adopt plateau to schedule the learning rate: if the development WER does not decrease for 6 evaluation steps, the learning rate will be decreased by a factor of 0.7. But since CSL does not have an official dev split, we decrease the learning rate after the 15th and 25th epoch and per 5 epochs after the 30th epoch. The maximum number of training epochs is set to 60.

**4.2.4 Inference and Decoding.** Following [44], to match the training condition, we evenly select every  $\frac{1}{p_d}$ -th frame to drop during inference, where  $p_d$  is the dropping ratio. We adopt the beam search algorithm with a beam size of 10 for decoding.

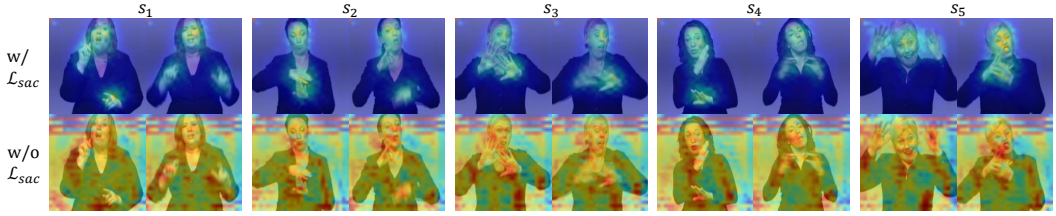


Fig. 7. Visualization results for learned spatial attention masks with or without the guidance of  $\mathcal{L}_{sac}$ . We randomly select five samples ( $s_1, \dots, s_5$ ) from the **test** set, and for each sample, we select one clear frame and one blurry frame. It is clear that the guidance of  $\mathcal{L}_{sac}$  can help the spatial attention module capture the informative regions (face and hands) more accurately.

Table 1. Ablation study for SAC and SEC. During inference, since our SEC can be removed, only the spatial attention module in SAC will introduce negligible parameters and affect inference speed. (SAC<sup>-</sup> denotes only inserting the spatial attention module but not guided by  $\mathcal{L}_{sac}$ ; Par.: number of parameters; Sp.: inference speed measured on the same TITAN RTX GPU in seconds per video.)

Backbone	SAC <sup>-</sup>	SAC	SEC	WER%	Par.(M)	Sp.(s)
VTB	✓	✓	✓	25.0	15.6359	0.169
				24.6	+0.0001	+0.002
				23.7	+0.0001	+0.002
				24.3	+0.0000	+0.000
				<b>22.6</b>	+0.0001	+0.002
CT	✓	✓	✓	26.1	8.7504	0.095
				26.0	+0.0001	+0.001
				25.1	+0.0001	+0.001
				25.2	+0.0000	+0.000
				<b>24.5</b>	+0.0001	+0.001
VLT	✓	✓	✓	21.5	16.1850	0.163
				21.4	+0.0001	+0.002
				20.8	+0.0001	+0.002
				20.9	+0.0000	+0.000
				<b>20.4</b>	+0.0001	+0.002

### 4.3 Ablation Studies for C<sup>2</sup>SLR

We first conduct ablation studies for C<sup>2</sup>SLR on PHOENIX-2014 following previous works [23, 43, 50, 75].

**4.3.1 Effectiveness of SAC and SEC.** As shown in Table 1, both SAC and SEC generalize well on different backbones: the performance of all the three backbones can be clearly improved. However, if the spatial attention module is inserted into the backbones without any guidance, *i.e.*, SAC<sup>-</sup>, the model performance can only be improved slightly, which verifies the effectiveness of  $\mathcal{L}_{sac}$ . The effectiveness of SEC suggests that explicitly enforcing the consistency between the visual and sequential modules at the sentence level can strengthen the cross-module cooperation, which leads to the performance gain. The improvements due to SAC and SEC are complementary so that using both of them can obtain better results than using only one of them. Besides, since VLT performs

Table 2. Ablation study for SAC.

Method	WER%	#Param(M)
VLT + SAC	<b>20.8</b>	16.1851
- channel weights	21.3	-0.0000
+ channel attention [65]	21.2	+0.0335
- post-processing	21.7	-0.0000
- face	21.1	-0.0000
- hands	21.2	-0.0000

the best among the three backbones, we will use it as the default backbone for the following experiments.

**4.3.2 Visualization Results for SAC.** Figure 7 shows the visualization results of the learned spatial attention masks of SAC (with  $\mathcal{L}_{sac}$ ) and SAC<sup>-</sup> (without  $\mathcal{L}_{sac}$ ) for five test samples. It should be noted that since SAC is deactivated during testing, our comparison is fair. First, it is quite clear that the learned attention masks with the guidance of  $\mathcal{L}_{sac}$  look much better. Without the guidance of  $\mathcal{L}_{sac}$ , the attention masks are quite messy with horizontal lines at the top and many highlights at trivial regions, e.g., the left shoulder of  $s_2$ , the hair of  $s_1$  and  $s_4$ , and the waist of  $s_3, s_5$ . This explains why SAC<sup>-</sup> can only slightly improve the performance of the backbones as shown in Table 1. Second, our SAC is so robust that the IRs (face and hands) in blurry frames (right columns of  $s_1$  to  $s_5$ ) can still be captured precisely. Third, it is capable of dealing with different hand positions: e.g., both two hands are lower than the face ( $s_1, s_3$ ); one hand is near the face while the other one is not ( $s_1, s_2, s_4$ ), and hands are overlapped ( $s_5$ ).

**4.3.3 Channel Weights.** Within our spatial attention module, each channel can receive a weight to better measure its importance before squeezing the feature maps. Removing the channel weights degenerates to the channel-wise average pooling in CBAM [65] and achieves a WER of 21.3%, which leads to a performance drop by 0.5% as shown in Table 2. Although our channel weights share a similar idea with the channel attention module of CBAM, which builds extra linear layers to generate the attention weights, no extra parameters are introduced in our spatial attention module. To further validate their effectiveness, after removing the channel weights, we conduct one more experiment by adding the channel attention module back as CBAM; however, it can only lead to a slight performance gain and cannot beat ours even with extra parameters.

**4.3.4 Heatmap Refinement.** We discuss in the Section 3.2.3 that the raw heatmaps of HRNet [58] consist of too many defects which may hinder the learning of the spatial attention module. As shown in Table 2, the quality of the keypoints heatmaps can make a difference on model performance: directly using the original heatmaps without post-processing achieves a WER of 21.7%, which reduces the performance of SAC by almost 1%.

**4.3.5 Effect of Each Informative Region.** As shown in the last two rows in Table 2, removing either face or hands region can harm the performance of SAC. The results validate that both signers' face and hands play a key role in conveying information, which is also mentioned in [32, 75].

**4.3.6 Effect of the Hyper-parameters  $\gamma_x, \gamma_y$  of Eq. 5.** We think  $\gamma_x$  and  $\gamma_y$  are two important hyper-parameters since they control the scale of highlighted regions in keypoints heatmaps. Thus, we conduct experiments to compare the performance of different  $\gamma_x, \gamma_y$  as shown in Figure 8. The model performance is worse when they are either too large (cannot cover the informative regions

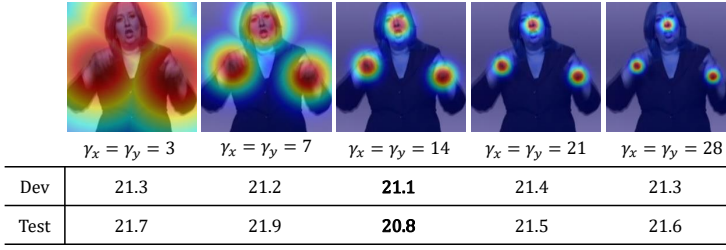


Fig. 8. Visualization results and performance comparison for different  $\gamma_x, \gamma_y$  in Eq. 5. Since for real practice, the height and the width of the spatial attention masks are usually the same, we set  $\gamma_x$  and  $\gamma_y$  to the same value.

Table 3. Ablation study for SEC.

(a) Ablation study for the architecture of the sentence embedding extractor and negative sampling. (TF: Transformer; DTCN: depth-wise TCN; Neg. Sam.: negative sampling.)

Method	Extractor	Neg. Sam.	WER%
VLT + SEC	TF+DTCN	✓	<b>20.9</b>
	TF+DTCN	×	21.5
	TF	✓	21.1
	BiLSTM	✓	21.3

(b) Ablation study for the constraint level. We fine-tune the loss factor of VA as [43] on the VLT for fair comparisons.

Level	Constraint	WER%
Sentence	consistency	<b>20.9</b>
Frame	consistency	21.6
	visual enhancement (VE) [43]	22.3
	visual alignment (VA) [43]	21.9
	VE+VA [43]	22.8

entirely) or too small (cover too many trivial regions). When  $\gamma_x = \gamma_y = 14$ , the model achieves the best performance.

**4.3.7 Sentence Embedding Extractor and Negative Sampling.** Our sentence embedding extractor consists of a depth-wise TCN layer and a transformer encoder aiming to model local and global contexts, respectively. As shown in Table 3a, local contexts are important to sentence embedding extraction as dropping the TCN layer would lead to worse performance. We also compare our method with the common practice, which concatenates the last two hidden states of BiLSTM and treats it as the sentence embedding. Nevertheless, that it underperforms the transformer-based extractors implies the strength of the self-attention mechanism for sentence embedding extraction. Table 3a also shows that negative sampling plays a key role in our SEC: without negative sampling, that is, directly minimizing the sentence embedding distance between the visual and sequential features, is not effective.

**4.3.8 Constraint Level.** As shown in Table 3b, we implement some frame-level constraints to validate the effectiveness of our SEC. First, we replace the sentence embeddings,  $\mathbf{v}_{se}$  and  $\mathbf{s}_{se}$  in Eq. 10, by their corresponding frame-level features to minimize the positive distances while maximizing the negative distances at the frame level. However, it leads to a performance degradation of 0.7% compared to our SEC. We further compare our SEC with VAC [43], which is composed of two frame-level constraints: visual enhancement (VE) and visual alignment (VA). First, an extra classifier is appended to the visual module to yield frame-level probability distributions (visual distribution). VE is implemented as a CTC loss computed between the visual distribution and the gloss label, which is the same as the one used for training the backbone. Second, VA is simply a KL-divergence loss,





Fig. 9. Two examples of video-gloss pairs.

Table 4. Examples of sentence embedding distances of the visual and sequential features.  $v_1$  and  $v_2$  are the videos in Figure 9.

$d(\cdot, \cdot)$	$\mathbf{E}_{sen}^s(v_1)$	$\mathbf{E}_{sen}^s(v_2)$
$\mathbf{E}_{sen}^v(v_1)$	0.01	1.99
$\mathbf{E}_{sen}^v(v_2)$	1.76	0.37

Table 5. Effect of the value of  $\lambda$  in Eq. 19.

$\lambda$	0	0.25	0.5	0.75	1.0	1.25	1.5
Dev	34.3	35.1	35.3	<b>33.1</b>	33.5	35.0	34.4
Test	34.4	33.8	33.1	<b>32.7</b>	32.8	34.2	33.6

which aims to minimize the distance between the visual distribution and the original probability distribution ( $p(\phi_i|\mathbf{x})$  in Eq. 16). Table 3b shows that both VE and VA perform much worse than our SEC. The results suggest that our SEC is a more proper way to measure the consistency between the visual and sequential modules.

**4.3.9 Examples of Video-gloss Pairs.** To verify whether  $\mathcal{L}_{sec}$  can really separate positive and negative samples, we provide two examples of video-gloss pairs denoted as  $(v_1, l_1)$  and  $(v_2, l_2)$  as shown in Figure 9. The sentence embedding distances of the visual and sequential features of  $v_1$  and  $v_2$  are shown in Table 4. It is clear that the distance between the two features of the same video (diagonal entries, positive pairs) can be very small. Otherwise (off-diagonal entries, negative pairs), the distance can be very large (the maximum value is 2.00).

#### 4.4 Ablation Studies for the Signer Removal Module

We further conduct ablation studies for our signer removal module (SRM) on the challenging signer-independent dataset, PHOENIX-2014-SI.

**4.4.1 Effect of the Hyper-parameter  $\lambda$  of Eq. 19.** According to [41], the weight for the domain classification loss, *i.e.*, our signer classification loss  $\mathcal{L}_{srm}$ , is an important hyper-parameter. We fine-tune it from 0 to 1.5 with an interval of 0.25 as shown in Table 5. When  $\lambda = 0$ , the model degenerates to  $C^2$ SLR and performs worse than other models with  $\lambda > 0$ . The results suggest the importance of removing signer information for SI-CSLR. When  $\lambda = 0.75$ , the model can achieve the best performance with a WER of 33.1%/32.7% on the dev and test set, respectively.

**4.4.2 Statistics Pooling and Gradient Reversal.** We further conduct ablation studies for the two major components of our SRM, the statistics pooling (SP) and gradient reversal (GR) layer. First, the use of the GR layer decides the type of learning method: feature disentanglement or multi-task learning. As shown in Table 6, it is clear that with the use of GR, models under the feature disentanglement setting can significantly outperform those under the multi-task learning setting.

Table 6. Ablation study for the signer removal module. (SP: statistics pooling; GR: gradient reversal)

Method	$\mathcal{L}_{srm}$	SP	GR	WER%	Type
				34.4	N/A
C <sup>2</sup> SLR+	✓			34.9	Multi-task Learning
	✓	✓		33.5	
	✓		✓	33.6	Feature Disentanglement
	✓	✓	✓	<b>32.7</b>	

Table 7. Performance comparison between seen and unseen signers.

Method	Seen Signers (WER%)	Unseen Signers (WER%)	Relative Gap (%)
C <sup>2</sup> SLR	22.7	34.4	51.5
C <sup>2</sup> SLR + SRM	23.0	32.7	<b>42.2</b>

The result implies that removing signer information is effective to SI-CSLR. However, we find that the model, C<sup>2</sup>SLR+SP, can also outperform the baseline under the multi-task setting. We think this is because the multi-task learning can be seen as a kind of regularization [72], which endows the shared networks between the CSLR and signer classification branches with better generalization capability. Similar ideas also appear in some works that jointly train a speech recognition model and a speaker recognition model [39, 49]. Finally, the effectiveness of SP also validates that sentence-level signer embeddings are more robust than frame-level ones to achieve signer classification, leading to better performance.

**4.4.3 Effect of the SRM over Seen and Unseen Signers.** We finally study the effect of the SRM over seen and unseen signers. We first build an extra test set consisting of only seen signers during training by removing videos performed by unseen signers from the official test set of PHOENIX-2014, and then retest “C<sup>2</sup>SLR” and “C<sup>2</sup>SLR+SRM” on this extra test set. As shown in Table 7, with a comparable performance over the seen signers, adding the SRM can significantly narrow the performance gap between unseen and seen signers. The results suggest that our SRM can be more helpful for the real-world situation that most testing signers are unseen.

## 4.5 Comparison with State-of-the-art Results

**4.5.1 Signer-dependent.** As shown in Table 8, we first evaluate our C<sup>2</sup>SLR on three signer-dependent benchmarks: PHOENIX-2014, PHOENIX-2014-T, and CSL-Daily.

Our C<sup>2</sup>SLR follows the idea of auxiliary learning, which also appears in some existing works, e.g., FCN [13] and VAC [43]. FCN proposes a gloss feature enhancement (GFE) module to introduce auxiliary supervision signals into the model training process. However, the GFE module highly relies on pseudo labels (CTC decoded results), which may contain too many errors. Our method only relies on pre-extracted heatmaps, which are quite accurate with the help of our post-processing algorithm, and the model’s inherent consistency: the visual and sequential features represent the same sentence. These two properties enable our method to outperform FCN by more than 3% on both PHOENIX-2014 and PHOENIX-2014-T. Recently, VAC proposes two auxiliary losses at the frame-level, which are not quite appropriate and perform worse than ours according to the

Table 8. Comparison on signer-dependent datasets. (R: RGB; F: optical flow; P: pose.)

Method	End-to-end	Modalities		PHOENIX-2014		PHOENIX-2014-T		CSL-Daily	
		Training	Inference	Dev	Test	Dev	Test	Dev	Test
CNN-LSTM-HMMs [33]	×	R	R	26.0	26.0	22.1	24.1	–	–
DNF (RGB) [15] + SBD-RL [64]	×	R	R	23.4	23.5	–	–	–	–
DNF [15]	×	R+F	R+F	23.1	22.9	–	–	32.8	32.4
CMA [50]	×	R	R	21.3	21.9	–	–	–	–
SMKD [23]	×	R	R	20.8	21.0	20.8	22.4	–	–
STMC [75]	×	R+P	R	21.1	20.7	19.6	21.0	–	–
SubUNets [4]	✓	R	R	40.8	40.7	–	–	41.4	41.0
LS-HAN [27]	✓	R	R	–	38.3	–	–	39.0	39.4
TIN + Transformer [73]	✓	R	R	–	–	–	–	33.6	33.1
SFL [44]	✓	R	R	24.9	25.3	25.1	26.1	–	–
FCN [13]	✓	R	R	23.7	23.9	23.3	25.1	33.2	32.5
SLT [6]	✓	R	R	–	–	24.6	24.5	33.1	32.0
VAC [43]	✓	R	R	21.2	22.3	–	–	–	–
MMTLB [12]	✓	R	R	–	–	21.9	22.5	–	–
C <sup>2</sup> SLR (ours)	✓	R+P	R	<b>20.5</b>	<b>20.4</b>	<b>20.2</b>	<b>20.4</b>	<b>31.9</b>	<b>31.0</b>

comparison in Section 4.3.8. The SOTA work, STMC [75], adopts the complicated stage optimization strategy, which introduces extra hyper-parameters, and needs to manually decide when to switch to a new stage. Our method is totally end-to-end trainable, and it can outperform STMC on both PHOENIX-2014 and PHOENIX-2014-T. To the best of our knowledge, this is the first time that an end-to-end method can outperform those using the stage optimization strategy.

In terms of modality usage, our method just uses extra pose modality during training, while only RGB videos are needed for inference. Thus, it is simpler for real application compared to DNF [15] which is built on a two-stream architecture taking both RGB videos and optical flow as inputs.

Finally, the results reported on CSL-Daily may be more important due to its large vocabulary size. Our method can still achieves SOTA performance on this large-scale dataset, which also validates the generalization capability of our method over different sign languages.

**4.5.2 Signer-independent.** As shown in Table 9, we further evaluate our SRM on the following two signer-independent benchmarks: PHOENIX-2014-SI and CSL.

Although some works, e.g., DNF [15] and CMA [50], evaluate their method on PHOENIX-2014-SI, none of them propose any dedicated module to deal with the challenging SI setting. In this work, we develop a simple yet effective signer removal module (SRM) for SI-CSLR to make the model more robust to signer discrepancy. As shown in Table 9a, our C<sup>2</sup>SLR can already achieve competitive performance on PHOENIX-2014-SI, and the SRM can further improve the performance significantly. The result validates that feature disentanglement is an effective method to remove signer-relevant information, and we believe our SRM can serve as a strong baseline for future works on SI-CSLR.

As shown in Table 9b, our SRM can lead to a relative performance gain of 24.4% over the baseline C<sup>2</sup>SLR on CSL<sup>5</sup>. It is worth noting that the SOTA work, MSeqGraph [59], uses three modalities including RGB, pose, and depth. However, our method only uses RGB and pose information for training, and only RGB frames are needed for inference. Thus, with a comparable performance to the SOTA work, we believe our method is more applicable in real practice.

<sup>5</sup>Although the SI setting itself is challenging, since the sentences in the CSL test set all appear in the training stage, the WER can be very low (< 1%).

Table 9. Comparison on signer-independent datasets. (R: RGB; F: optical flow; P: pose; D: depth.)

(a) PHOENIX-2014-SI.

Method	End-to-end	Modalities		Dev	Test
		Training	Inference		
Re-sign [35]	×	R	R	45.1	44.1
DNF [15]	×	R+F	R+F	36.0	35.7
CMA [50]	×	R	R	34.8	34.3
C <sup>2</sup> SLR (ours)	✓	R+P	R	34.3	34.4
C <sup>2</sup> SLR + SRM (ours)	✓	R+P	R	<b>33.1</b>	<b>32.7</b>

(b) CSL.

Method	End-to-end	Modalities		Test
		Training	Inference	
LS-HAN [27]	×	R	R	17.3
DPD + TEM [74]	×	R	R	4.7
STMC [75]	×	R+P	R	2.1
CTF [63]	✓	R	R	11.2
HLSTM-attn [22]	✓	R	R	10.2
FCN [13]	✓	R	R	3.0
VAC [43]	✓	R	R	1.6
MSeqGraph [59]	✓	R+P+D	R+P+D	0.6
C <sup>2</sup> SLR (ours)	✓	R+P	R	0.90
C <sup>2</sup> SLR + SRM (ours)	✓	R+P	R	0.68

## 5 CONCLUSION

In this work, we enhance CSLR backbones by developing three auxiliary tasks. First, we insert a keypoint-guided spatial attention module into the visual module to enforce the visual module to focus on informative regions. Second, we impose a sentence embedding consistency constraint between the visual and sequential features to enhance the representation power of both features. We conduct proper ablation studies to validate the effectiveness of the two consistency constraints both quantitatively and qualitatively. Finally, on top of the consistency-enhanced CSLR backbone, a signer removal module based on feature disentanglement is proposed for signer-independent CSLR. More remarkably, our model can achieve SOTA or competitive performance on five benchmarks, while the whole model is trained in an end-to-end manner.

## ACKNOWLEDGMENTS

The work described in this paper was supported by a grant from the Research Grants Council of the Hong Kong Special Administrative Region, China (Project No. HKUST16200118)

## REFERENCES

- [1] Nikolaos M. Adaloglou, Theodoros Chatzis, Ilias Papastratis, Andreas Stergioulas, Georgios Th Papadopoulos, Vassia Zacharopoulou, George Xydopoulos, Klimis Antzakas, Dimitris Papazachariou, and Petros Daras. 2021. A Comprehensive Study on Deep Learning-based Methods for Sign Language Recognition. *IEEE TMM* (2021), 1–1.

- [2] Mykhaylo Andriluka, Leonid Pishchulin, Peter Gehler, and Bernt Schiele. 2014. 2D Human Pose Estimation: New benchmark and State of the Art Analysis. In *CVPR*. 3686–3693.
- [3] Jimmy Lei Ba, Jamie Ryan Kiros, and Geoffrey E. Hinton. 2016. Layer Normalization. *arXiv preprint arXiv:1607.06450* (2016).
- [4] Necati Cihan Camgöz, Simon Hadfield, Oscar Koller, and Richard Bowden. 2017. SubUNets: End-to-End Hand Shape and Continuous Sign Language Recognition. In *ICCV*. 3075–3084.
- [5] Necati Cihan Camgoz, Simon Hadfield, Oscar Koller, Hermann Ney, and Richard Bowden. 2018. Neural Sign Language Translation. In *CVPR*.
- [6] Necati Cihan Camgöz, Oscar Koller, Simon Hadfield, and Richard Bowden. 2020. Sign Language Transformers: Joint End-to-End Sign Language Recognition and Translation. In *CVPR*. 10020–10030.
- [7] Yue Cao, Jiarui Xu, Stephen Lin, Fangyun Wei, and Han Hu. 2019. GCNet: Non-local Networks Meet Squeeze-excitation Networks and Beyond. In *CVPRW*.
- [8] Zhe Cao, Gines Hidalgo, Tomas Simon, Shih-En Wei, and Yaser Sheikh. 2019. OpenPose: Realtime Multi-person 2D Pose Estimation using Part Affinity Fields. *TPAMI* 43, 1 (2019), 172–186.
- [9] Fredrik Carlsson, Amaru Cuba Gyllensten, Evangelia Gogoulou, Erik Ylipää Hellqvist, and Magnus Sahlgren. 2020. Semantic Re-tuning with Contrastive Tension. In *ICLR*.
- [10] Joao Carreira, Eric Noland, Andras Banki-Horvath, Chloe Hillier, and Andrew Zisserman. 2018. A Short Note about Kinetics-600. *arXiv preprint arXiv:1808.01340* (2018).
- [11] Shaoxiang Chen and Yu-Gang Jiang. 2019. Motion Guided Spatial Attention for Video Captioning. In *AAAI*, Vol. 33. 8191–8198.
- [12] Yutong Chen, Fangyun Wei, Xiao Sun, Zhirong Wu, and Stephen Lin. 2022. A Simple Multi-modality Transfer Learning Baseline for Sign Language Translation. In *CVPR*. 5120–5130.
- [13] Ka Leong Cheng, Zhaoyang Yang, Qifeng Chen, and Yu-Wing Tai. 2020. Fully Convolutional Networks for Continuous Sign Language Recognition. In *ECCV*, Vol. 12369. 697–714.
- [14] Yihua Cheng, Yiwei Bao, and Feng Lu. 2022. PureGaze: Purifying Gaze Feature for Generalizable Gaze Estimation. In *AAAI*.
- [15] Rumpeng Cui, Hu Liu, and Changshui Zhang. 2019. A Deep Neural Framework for Continuous Sign Language Recognition by Iterative Training. *IEEE TMM PP* (07 2019), 1–1.
- [16] Jun Fu, Jing Liu, Haijie Tian, Yong Li, Yongjun Bao, Zhiwei Fang, and Hanqing Lu. 2019. Dual Attention Network for Scene Segmentation. In *CVPR*. 3146–3154.
- [17] Yaroslav Ganin, Evgeniya Ustinova, Hana Ajakan, Pascal Germain, Hugo Larochelle, François Laviolette, Mario Marchand, and Victor Lempitsky. 2016. Domain-adversarial Training of Neural Networks. *JMLR* 17, 1 (2016), 2096–2030.
- [18] Tianyu Gao, Xingcheng Yao, and Danqi Chen. 2021. SimCSE: Simple Contrastive Learning of Sentence Embeddings. *EMNLP* (2021).
- [19] Raghav Goyal, Samira Ebrahimi Kahou, Vincent Michalski, Joanna Materzynska, Susanne Westphal, Heuna Kim, Valentin Haenel, Ingo Fruend, Peter Yianilos, Moritz Mueller-Freitag, et al. 2017. The “something something” Video Database for Learning and Evaluating Visual Common Sense. In *ICCV*. 5842–5850.
- [20] Alex Graves, Santiago Fernández, Faustino Gomez, and Jürgen Schmidhuber. 2006. Connectionist Temporal Classification: Labelling Unsegmented Sequence Data with Recurrent Neural Networks. In *ICML*. 369–376.
- [21] Dan Guo, Shuo Wang, Qi Tian, and Meng Wang. 2019. Dense Temporal Convolution Network for Sign Language Translation. In *IJCAI*. 744–750.
- [22] Dan Guo, Wengang Zhou, Houqiang Li, and Meng Wang. 2018. Hierarchical LSTM for Sign Language Translation. In *AAAI*. 6845–6852.
- [23] Aiming Hao, Yuecong Min, and Xilin Chen. 2021. Self-Mutual Distillation Learning for Continuous Sign Language Recognition. In *ICCV*. 11303–11312.
- [24] R Devon Hjelm, Alex Fedorov, Samuel Lavoie-Marchildon, Karan Grewal, Phil Bachman, Adam Trischler, and Yoshua Bengio. 2019. Learning Deep Representations by Mutual Information Estimation and Maximization. In *ICLR*.
- [25] Hezhen Hu, Wengang Zhou, Junfu Pu, and Houqiang Li. 2021. Global-local Enhancement Network for NMF-aware Sign Language Recognition. *ACM TOMM* 17, 3 (2021), 1–19.
- [26] Jie Hu, Li Shen, Samuel Albanie, Gang Sun, and Andrea Vedaldi. 2018. Gather-Excite: Exploiting Feature Context in Convolutional Neural Networks. *NeurIPS* 31 (2018), 9401–9411.
- [27] Jie Huang, Wengang Zhou, Qilin Zhang, Houqiang Li, and Weiping Li. 2018. Video-Based Sign Language Recognition Without Temporal Segmentation. In *AAAI*. 2257–2264.
- [28] Zhizhong Huang, Junping Zhang, and Hongming Shan. 2021. When Age-invariant Face Recognition Meets Face Age Synthesis: A Multi-task Learning Framework. In *CVPR*. 7282–7291.

- [29] Xin Jin, Cuiling Lan, Wenjun Zeng, Zhibo Chen, and Li Zhang. 2020. Style Normalization and Restitution for Generalizable Person Re-identification. In *CVPR*. 3143–3152.
- [30] Jacob Devlin Ming-Wei Chang Kenton and Lee Kristina Toutanova. 2019. BERT: Pre-training of Deep Bidirectional Transformers for Language Understanding. In *NAACL-HLT*. 4171–4186.
- [31] Diederik P. Kingma and Jimmy Ba. 2015. Adam: A Method for Stochastic Optimization. In *ICLR*.
- [32] Oscar Koller. 2020. Quantitative Survey of the State of the Art in Sign Language Recognition. *arXiv preprint arXiv:2008.09918* (2020).
- [33] Oscar Koller, Necati Camgoz, Hermann Ney, and Richard Bowden. 2019. Weakly Supervised Learning with Multi-Stream CNN-LSTM-HMMs to Discover Sequential Parallelism in Sign Language Videos. *IEEE TPAMI* 42, 9 (04 2019), 2306–2320.
- [34] Oscar Koller, Jens Forster, and Hermann Ney. 2015. Continuous Sign Language Recognition: Towards Large Vocabulary Statistical Recognition Systems Handling Multiple Signers. *CVIU* 141 (Dec. 2015), 108–125.
- [35] Oscar Koller, Sepehr Zargaran, and Hermann Ney. 2017. Re-Sign: Re-Aligned End-to-End Sequence Modelling with Deep Recurrent CNN-HMMs. In *CVPR*. 3416–3424.
- [36] Oscar Koller, Sepehr Zargaran, Hermann Ney, and Richard Bowden. 2018. Deep Sign: Enabling Robust Statistical Continuous Sign Language Recognition via Hybrid CNN-HMMs. *IJCV* 126, 12 (2018), 1311–1325.
- [37] Xingze Li, Wengang Zhou, Yun Zhou, and Houqiang Li. 2020. Relation-guided Spatial Attention and Temporal Refinement for Video-based Person Re-identification. In *AAAI*, Vol. 34. 11434–11441.
- [38] Drew Linsley, Dan Shiebler, Sven Eberhardt, and Thomas Serre. 2018. Learning What and Where to Attend. In *ICLR*.
- [39] Yi Liu, Liang He, Jia Liu, and Michael T Johnson. 2018. Speaker Embedding Extraction with Phonetic Information. *Interspeech* (2018), 2247–2251.
- [40] Yue Liu, Xin Wang, Yitian Yuan, and Wenwu Zhu. 2019. Cross-modal Dual Learning for Sentence-to-video Generation. In *ACM MM*. 1239–1247.
- [41] Yu Liu, Fangyin Wei, Jing Shao, Lu Sheng, Junjie Yan, and Xiaogang Wang. 2018. Exploring Disentangled Feature Representation beyond Face Identification. In *CVPR*. 2080–2089.
- [42] Thang Luong, Hieu Pham, and Christopher D. Manning. 2015. Effective Approaches to Attention-based Neural Machine Translation. In *EMNLP*. 1412–1421.
- [43] Yuecong Min, Aiming Hao, Xiujuan Chai, and Xilin Chen. 2021. Visual Alignment Constraint for Continuous Sign Language Recognition. In *ICCV*. 11542–11551.
- [44] Zhe Niu and Brian Mak. 2020. Stochastic Fine-Grained Labeling of Multi-state Sign Glosses for Continuous Sign Language Recognition. In *ECCV*. 172–186.
- [45] Aaron van den Oord, Yazhe Li, and Oriol Vinyals. 2018. Representation Learning with Contrastive Predictive Coding. *arXiv preprint arXiv:1807.03748* (2018).
- [46] Hamid Palangi, Li Deng, Yelong Shen, Jianfeng Gao, Xiaodong He, Jianshu Chen, Xinying Song, and Rabab Ward. 2016. Deep Sentence Embedding using Long Short-term Memory Networks: Analysis and Application to Information Retrieval. *IEEE/ACM TASLP* 24, 4 (2016), 694–707.
- [47] Yanwei Pang, Jin Xie, Muhammad Haris Khan, Rao Muhammad Anwer, Fahad Shahbaz Khan, and Ling Shao. 2019. Mask-guided Attention Network for Occluded Pedestrian Detection. In *CVPR*. 4967–4975.
- [48] Katerina Papadimitriou and Gerasimos Potamianos. 2020. Multimodal Sign Language Recognition via Temporal Deformable Convolutional Sequence Learning. In *Interspeech*. 2752–2756.
- [49] Gueorgui Pironkov, Stéphane Dupont, and Thierry Dutoit. 2016. Speaker-aware Long Short-term Memory Multi-task Learning for Speech Recognition. In *European Signal Processing Conference (EUSIPCO)*. 1911–1915.
- [50] Junfu Pu, Wengang Zhou, Hezhen Hu, and Houqiang Li. 2020. Boosting Continuous Sign Language Recognition via Cross Modality Augmentation. In *ACM MM*. 1497–1505.
- [51] Junfu Pu, Wengang Zhou, and Houqiang Li. 2018. Dilated Convolutional Network with Iterative Optimization for Continuous Sign Language Recognition. In *IJCAI*. 885–891.
- [52] Junfu Pu, Wengang Zhou, and Houqiang Li. 2019. Iterative Alignment Network for Continuous Sign Language Recognition. In *CVPR*. 4165–4174.
- [53] Nils Reimers and Iryna Gurevych. 2019. Sentence-BERT: Sentence Embeddings using Siamese BERT-Networks. In *EMNLP*. 3982–3992.
- [54] Florian Schroff, Dmitry Kalenichenko, and James Philbin. 2015. Facenet: A Unified Embedding for Face Recognition and Clustering. In *CVPR*. 815–823.
- [55] Peter Shaw, Jakob Uszkoreit, and Ashish Vaswani. 2018. Self-Attention with Relative Position Representations. In *NAACL-HLT*. 464–468.
- [56] Karen Simonyan and Andrew Zisserman. 2015. Very Deep Convolutional Networks for Large-Scale Image Recognition. In *ICLR*.

- [57] David Snyder, Daniel Garcia-Romero, Gregory Sell, Daniel Povey, and Sanjeev Khudanpur. 2018. X-vectors: Robust DNN Embeddings for Speaker Recognition. In *ICASSP*. 5329–5333.
- [58] Ke Sun, Bin Xiao, Dong Liu, and Jingdong Wang. 2019. Deep High-resolution Representation Learning for Human Pose Estimation. In *CVPR*. 5693–5703.
- [59] Shengeng Tang, Dan Guo, Richang Hong, and Meng Wang. 2021. Graph-Based Multimodal Sequential Embedding for Sign Language Translation. *IEEE TMM* (2021).
- [60] Ashish Vaswani, Noam Shazeer, Niki Parmar, Jakob Uszkoreit, Llion Jones, Aidan N. Gomez, Lukasz Kaiser, and Illia Polosukhin. 2017. Attention is All you Need. In *NeurIPS*. 5998–6008.
- [61] Fei Wang, Mengqing Jiang, Chen Qian, Shuo Yang, Cheng Li, Honggang Zhang, Xiaogang Wang, and Xiaoou Tang. 2017. Residual Attention Network for Image Classification. In *CVPR*. 3156–3164.
- [62] Jindong Wang, Cuiling Lan, Chang Liu, Yidong Ouyang, Wenjun Zeng, and Tao Qin. 2021. Generalizing to Unseen Domains: A Survey on Domain Generalization. *arXiv preprint arXiv:2103.03097* (2021).
- [63] Shuo Wang, Dan Guo, Wen-gang Zhou, Zheng-Jun Zha, and Meng Wang. 2018. Connectionist Temporal Fusion for Sign Language Translation. In *ACM MM*. 1483–1491.
- [64] Chengcheng Wei, Jian Zhao, Wengang Zhou, and Houqiang Li. 2020. Semantic Boundary Detection with Reinforcement Learning for Continuous Sign Language Recognition. *IEEE TCSVT* 31, 3 (2020), 1138–1149.
- [65] Sanghyun Woo, Jongchan Park, Joon-Young Lee, and In So Kweon. 2018. CBAM: Convolutional Block Attention Module. In *ECCV*. 3–19.
- [66] Felix Wu, Angela Fan, Alexei Baevski, Yann Dauphin, and Michael Auli. 2018. Pay Less Attention with Lightweight and Dynamic Convolutions. In *ICLR*.
- [67] Tian Xu, Jennifer White, Sinan Kalkan, and Hatice Gunes. 2020. Investigating Bias and Fairness in Facial Expression Recognition. In *ECCV*. 506–523.
- [68] Baosong Yang, Zhaopeng Tu, Derek F. Wong, Fandong Meng, Lidia S. Chao, and Tong Zhang. 2018. Modeling Localness for Self-Attention Networks. In *EMNLP*. 4449–4458.
- [69] Mang Ye, Xu Zhang, Pong C Yuen, and Shih-Fu Chang. 2019. Unsupervised Embedding Learning via Invariant and Spreading Instance Feature. In *CVPR*. 6210–6219.
- [70] Fang Yin, Xiujuan Chai, and Xilin Chen. 2016. Iterative Reference Driven Metric Learning for Signer Independent Isolated Sign Language Recognition. In *ECCV*. 434–450.
- [71] Adams Wei Yu, David Dohan, Minh-Thang Luong, Rui Zhao, Kai Chen, Mohammad Norouzi, and Quoc V. Le. 2018. QANet: Combining Local Convolution with Global Self-Attention for Reading Comprehension. In *ICLR*.
- [72] Yu Zhang and Qiang Yang. 2021. A Survey on Multi-task Learning. *IEEE TKDE* (2021).
- [73] Hao Zhou and et al. 2021. Improving Sign Language Translation with Monolingual Data by Sign Back-Translation. In *CVPR*.
- [74] Hao Zhou, Wengang Zhou, and Houqiang Li. 2019. Dynamic Pseudo Label Decoding for Continuous Sign Language Recognition. In *ICME*. 1282–1287.
- [75] Hao Zhou, Wengang Zhou, Yun Zhou, and Houqiang Li. 2020. Spatial-Temporal Multi-Cue Network for Continuous Sign Language Recognition. In *AAAI*. 13009–13016.
- [76] Hao Zhou, Wengang Zhou, Yun Zhou, and Houqiang Li. 2021. Spatial-Temporal Multi-Cue Network for Sign Language Recognition and Translation. *IEEE TMM* (2021), 1–1.
- [77] Ronglai Zuo and Brian Mak. 2022. C2SLR: Consistency-Enhanced Continuous Sign Language Recognition. In *CVPR*. 5131–5140.

Received 20 February 2007; revised 12 March 2009; accepted 5 June 2009